Available online at www.sciencedirect.com
SCIENCE DIRECT®
International Journal of Heat and Mass Transfer 48 (2005) 4598–4614
International Journal of HEAT and MASS TRANSFER
www.elsevier.com/locate/ijhmt

Flow and heat transfer across a confined square cylinder in the steady flow regime: Effect of Peclet number

A.K. Dhiman [a], R.P. Chhabra [a,*], V. Eswaran [b]

[a] Department of Chemical Engineering, Indian Institute of Technology, Kanpur 208 016, India
[b] Department of Mechanical Engineering, Indian Institute of Technology, Kanpur 208 016, India

Received 17 September 2004; received in revised form 1 February 2005
Available online 21 July 2005

Abstract

The flow and heat transfer characteristics of an isolated square cylinder in crossflow placed symmetrically in a planar slit have been investigated for the range of conditions as $1 \leqslant Re \leqslant 45$, $0.7 \leqslant Pr \leqslant 4000$ ($Pe \leqslant 4000$) and $\beta = 1/8$, $1/6$ and $1/4$. Heat transfer correlations have been obtained in the steady flow regime for the constant temperature and constant heat flux boundary conditions on the solid square cylinder in crossflow. In addition, variation of the local Nusselt number on each face of the obstacle and representative isotherm plots are presented to elucidate the role of Prandtl number and blockage ratio on drag coefficient and heat transfer.

Keywords: Steady flow; Blockage ratio; Peclet number; Square cylinder; Nusselt number

1. Introduction

In recent years, considerable interest has been shown in studying the flow of Newtonian fluids past cylinders of circular and square cross-section oriented normal to the direction of flow. Such studies have received impetus from theoretical considerations, because of the wide variety of fluid flow phenomena associated with such idealized shapes as well as from pragmatic considerations, since a reliable knowledge of engineering parameters (drag coefficient, Nusselt number, wake size, etc.) is frequently needed for the design of cooling towers, chimneys, antennas, support structures, etc. Consequently, over the years, a wealth of information has accumulated in the literature, most of which relates to circular cylinders. The bulk of the information related to hydrodynamic aspects of this problem has been reviewed recently [1,2] whereas the heat transfer aspects have been surveyed elsewhere [3,4]. However, unlike in the case of a circular cylinder, the separation points are fixed for a square cylinder, which thus presents a quite different case. Based on a combination of numerical and experimental studies, different flow regimes for the square cylinder have been identified in the literature depending upon the value of the Reynolds number [5–14]. The main flow regimes reported to date are: a creeping flow region in which no flow separation takes place at the surface of the cylinder ($Re \leqslant 1$). At low Reynolds numbers ($2 < Re < 60$), a closed steady recirculation region characterized by the formation of two symmetric vortices behind the bluff body is observed. A critical value of the Reynolds number seems to lie in the range 50–70, beyond which, a von Karman vortex street forms

* Corresponding author. Tel.: +91 512 259 7393; fax: +91 512 259 0104.
E-mail address: chhabra@iitk.ac.in (R.P. Chhabra).

0017-9310/$ - see front matter © 2005 Elsevier Ltd. All rights reserved.
doi:10.1016/j.ijheatmasstransfer.2005.04.033

Nomenclature

b	side of the square cylinder (m)
C_D	total drag coefficient (–) [$= F_D/(\frac{1}{2}\rho U_{max}^2 b)$]
C_{Df}	friction or viscous drag coefficient (–)
C_{DP}	pressure drag coefficient (–)
c_p	specific heat of the fluid (J/kg K)
CV	control volume
F_D	drag force on the cylinder (N/m)
F_{Df}	friction drag force on the cylinder (N/m)
F_{DP}	pressure drag force on the cylinder (N/m)
h	local convective heat transfer coefficient (W/m^2 K)
$\bar{h}$	average convective heat transfer coefficient (W/m^2 K)
j	Colburn factor for heat transfer (–) [$= Nu/(Re \times Pr^{1/3})$]
k	thermal conductivity of the fluid (W/m K)
L_1	length of the computational domain (m)
L_2	height of the computational domain (m)
L_r	recirculation length (m)
M	number of grid points in the x-direction
N	number of grid points in the y-direction
n	cylinder surface normal direction (–)
Nu	average Nusselt number of the cylinder (–) [$= \bar{h}b/k$]
Nu_f	average Nusselt number of the front surface of the cylinder (–)
Nu_L	local Nusselt number of the cylinder (–) [$= hb/k$]
Nu_r	average Nusselt number of the rear surface of the cylinder (–)
Nu_t	average Nusselt number of the top surface of the cylinder (–)
p	pressure (–) [$= p'/(\rho U_{max}^2)$]
Pe	Peclet number (–) [$= Re \times Pr$]
Pr	Prandtl number (–) [$= \mu c_p/k$]
q_w	heat flux (W/m^2)
Re	Reynolds number (–) [$= bU_{max}\rho/\mu$]
t	time (–) [$= t'/(b/U_{max})$]
T	temperature (–) [$= (T' - T_\infty)/(T'_w - T_\infty)$ or $(T' - T_\infty)/(q_w b/k)$]
T_∞	temperature of the fluid at the channel inlet (K)
T'_w	constant wall temperature at the surface of the cylinder (K)
u	component of the velocity in x-direction (–) [$= u'/U_{max}$]
U_c	average streamwise velocity (–)
U_{max}	maximum velocity of the fluid at the channel inlet (m/s)
v	component of the velocity in y-direction (–) [$= v'/U_{max}$]
x	streamwise coordinate (–) [x'/b]
X_d	downstream face distance of the cylinder from the outlet (m)
X_u	upstream face distance of the cylinder from the inlet (m)
y	transverse coordinate (–) [y'/b]

Greek symbols

β	blockage ratio (–) [$= b/L_2$]
δ	size of the CV clustered around the cylinder (m)
Δ	size of the CV far away from the cylinder in x-direction (m)
μ	dynamic viscosity of the fluid (Pa s)
Φ	dependent variable in convective boundary condition (–)
ρ	density of the fluid (kg/m^3)

Subscripts

∞	inlet condition
f	front face of the square cylinder
r	rear face of the square cylinder
t	top face of the square cylinder
w	surface of the square cylinder

Superscript

$'$	dimensional variable

in the flow field. When the Reynolds number is further increased ($100 \leqslant Re \leqslant 200$), the flow separates at the leading edges of the cylinder also, and beyond around $Re = 160$, the flow becomes three-dimensional in an unbounded flow, the onset of which is not fully investigated yet in the literature.

Obviously, not only the values of the engineering parameters, such as drag coefficient, Nusselt number, wake size, etc., vary from one regime to another but these also exhibit different dependence on the Reynolds and Peclet number. Furthermore, the kinematics of flow and the macroscopic engineering parameters are also influenced by the blockage ratio, i.e., the relative position of the bounding walls. This work sets out to elucidate the role of blockage ratio on the flow and heat transfer characteristics from a square cylinder over wide ranges of Peclet number in the steady two-dimensional flow regime. However, before undertaking a detailed presentation and discussion of this problem, it is useful to recount briefly the current status of the relevant literature.

2. Previous work

Most of the currently available literature on the incompressible fluid flow over square cylinder relates to the high Reynolds number region where the main thrust has been to investigate the wake phenomena, time dependent drag and lift characteristics, vortex shedding frequency, etc. In contrast, much less attention has been devoted to heat transfer characteristics. Davis et al. [15] investigated, both experimentally and numerically, the confined flow across a square cylinder for two blockage ratios ($\beta = 1/6$ and $1/4$) for a wide range of Reynolds number ($100 \leqslant Re \leqslant 1850$). They employed a finite volume method (FVM) on non-uniform grids of 51×28, 76×42 and 76×52 grid points and found that the presence of confining wall and the shape of the inflow velocity profile lead to numerous changes in the characteristics of the flow around the square cylinder in a channel. Mukhopadhyay et al. [16] carried out a 2D numerical investigation in the Reynolds number range 55.5–1200 at four blockage ratios ($\beta = 1/8$, $1/4$, $5/16$ and $100/267$) with a parabolic velocity field at the channel inlet and found the periodicity of the flow to be damped in the downstream region of a long duct due to the influence of channel walls. With increasing blockage effect, the value of Strouhal number was seen to increase. Suzuki and Suzuki [17] reported a numerical and experimental study for the confined flow obstructed by a square cylinder at constant temperature and at blockage ratios of 1/10, 1/5 and 50/167 for $Re = 50$, 100 and 150 (based on average velocity) for various inlet flow conditions in a channel. The flow was found to fluctuate in a highly periodic fashion and the Karman vortex formed downstream from the cylinder exhibited a crisscross motion in the confined channel flow. Valencia [18] studied the effect of a square cylinder on heat transfer from the heated channel with a uniform inflow profile at blockage ratios of 1/4 and 1/2 (corresponding to $Re = 50$–500) for air ($Pr = 0.71$) and reported significant enhancement in the values of Nusselt number due to the built-in obstacle. Bernsdorf et al. [19] simulated a 2D channel flow around a square obstacle for a range of Reynolds number between 80 and 300 and a blockage ratio of 1/8 using lattice-Boltzmann (BGK) automata. Strouhal numbers for time dependent, viscous, incompressible flows were estimated numerically. They also found that for a correct evaluation of the Strouhal number, higher grid resolutions are necessary for higher Reynolds numbers owing to the generation of small secondary vortices below and above the obstacle. Breuer et al. [5] carried out a 2D study for the confined flow around a square cylinder in a channel with FVM on non-equidistant staggered grids in the Reynolds number range $0.5 \leqslant Re \leqslant 300$ for a fixed blockage ratio of 1/8 with parabolic velocity profile at the channel inlet. Both steady ($0.5 \leqslant Re < 60$) and unsteady ($60 \leqslant Re \leqslant 300$) flows have been investigated. They found an excellent agreement between the computations of lattice-Boltzmann automata (LBA) and of FVM. The integral quantities such as drag coefficient, recirculation length and Strouhal number were evaluated. Guo et al. [6] also simulated the confined 2D flow around a square cylinder in the Reynolds number range $1 \leqslant Re \leqslant 500$ for a fixed blockage ratio of 1/8 by using non-uniform Lattice-BGK model. It was found that the periodicity of the flow was damped out for $Re > 300$. Turki et al. [20,21] have numerically studied the effect of three blockage ratios ($\beta = 1/8$, $1/6$ and $1/4$) on the 2D unsteady flow past a square cylinder inside horizontal channel for Reynolds number ranging from 62 to 300, and for the forced and mixed convection around a heated cylinder for blockage ratios of $\beta = 1/8$ and $1/4$ for Richardson number up to 0.1 in the Reynolds number range from 62 to 200 for air. The critical value of Reynolds number increases with the increasing blockage ratio, β in pure forced convection and it was found at $Re = 62$, 85 and 120 for $\beta = 1/8$, $1/6$ and $1/4$, respectively. In mixed convection, the critical value of Reynolds number decreases with increasing Richardson number while the Strouhal number increases with Richardson number. Finally, heat transfer correlations have been obtained for forced and mixed convection conditions. Many of these studies mentioned above are 2D, but it is well known that the flow becomes 3D at different values of the Reynolds number, Re which is strongly dependent on the degree of confinement. It is unclear if the 2D computations are always realistic for the Reynolds number ranges over which they have been applied in some of the aforementioned. Sharma and Eswaran [11–13] investigated the 2D steady and unsteady periodic flow across a square cylinder for both unconfined and confined channel flow with forced and mixed convection heat transfer. Their results encompass wide ranges of parameters as $1 \leqslant Re \leqslant 160$ and Richardson number $= 0$ to ± 1 for $Pr = 0.7$. The focus of these studies was towards understanding the onset and/or suppression of vortex shedding in the presence or absence of a channel and/or a buoyancy force. Recently, Gupta et al. [22] have investigated the 2D steady confined flow ($5 \leqslant Re \leqslant 40$; $\beta = 1/8$) of power law fluids past a square cylinder for a range of Peclet number 5–400 by using FDM on uniform staggered grid arrangement in a channel with parabolic velocity profile at the channel inlet. The shear-thinning behaviour not only reduces the size of the recirculation region but also delays the wake formation, and shear-thickening fluids show the opposite effect on the wake formation. They also found the faster decay in the temperature field at high Peclet numbers in shear-thinning fluids, with the reverse behaviour being observed in shear-thickening. Overall, shear-thinning fluid behaviour facilitates heat transfer whereas shear-thickening behaviour impedes it.

While it is readily acknowledged that the values of Prandtl number up to ~100 are frequently encountered in chemical, petroleum and oil related industrial applications, yet very little prior work is available on the effect of Prandtl number on the forced convection heat transfer characteristics from a square cylinder. Furthermore, owing to the generally high viscosity of process streams, the Reynolds numbers are not excessively high and the assumption of 2D steady flow is justified under these conditions. Dhiman et al. [23] have recently studied the effect of Peclet number ($0.7 < Pe < 4000$) on the heat transfer across a square cylinder in an unconfined domain in the steady flow regime ($1 \leqslant Re \leqslant 45$). However, no numerical results are available in the literature on the effects of Prandtl number on the heat transfer coefficients in the crossflow of Newtonian fluids past a square cylinder in the steady flow regime ($1 \leqslant Re \leqslant 45$) at different blockage ratios. Therefore, the main objective of the present work is to study the effect of Prandtl number on the flow and heat transfer characteristics of an isolated square cylinder in crossflow for the range of conditions as $1 \leqslant Re \leqslant 45$ and $0.7 \leqslant Pe \leqslant 4000$ and $\beta = 1/8$, 1/6 and 1/4. These results in turn have been used to develop heat transfer correlations for the constant temperature and constant heat flux boundary conditions prescribed on the solid square cylinder in crossflow configuration. The range of the values of Prandtl number varies from one Reynolds number to another such that the maximum value of the Peclet number is 4000 in this study. Thus, for instance, the maximum value of $Pr = 50$ was used for $Re = 45$. This is justified as highly viscous fluids will correspond to large values of Pr and small values of Re.

3. Geometrical configuration

The system of interest here is the confined flow of an incompressible fluid in a channel with a heated square cylinder placed symmetrically on the center-line (Fig. 1). The square cylinder with side b, also the non-dimensionalizing length scale, is exposed to a parabolic velocity field at the inlet, with the maximum value of velocity equal to U_{max}, and a constant temperature of T_∞ at the channel inlet. The aim is to simulate an infinitely long channel. However, as the computational domain has to be finite, the non-dimensional upstream distance between the inlet plane and the front surface of the cylinder, X_u/b, is taken as 8.5, and the non-dimensional downstream distance between the rear surface of the cylinder and the exit plane, X_d/b, is taken 16.5, with the total non-dimensional length of the computational domain $L_1/b = 26$ in the axial direction. In order to explore the influence of the assumed finite domain, especially for the lowest Reynolds number, computations have been carried out for $X_u/b = 10.5$ and 6.5 for $\beta = 1/8$ and 1/4 at $Re = 1$ for $X_d/b = 16.5$. The percentage change in the value of C_D for $X_u/b = 6.5$ and 8.5 is $< 0.012\%$ with respect to $X_u/b = 10.5$ for $\beta = 1/8$. This change in the value of C_D reduces to $<0.018\%$ for $\beta = 1/4$. These values of upstream and/or downstream distances are also in line with those used by others [9,11,13], and have been shown to give results that approach the asymptotic values for an infinite channel. The non-dimensional vertical distance between the upper and lower walls, L_2/b, defines the blockage ratio ($\beta = b/L_2$). Three values of the blockage ratio ($\beta = 1/8$, 1/6 and 1/4) have been used in this work. The choice of these values has been guided by the information available in the literature.

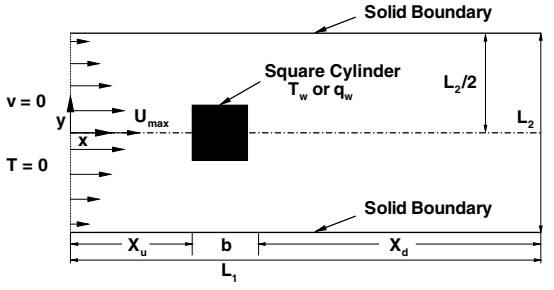

Fig. 1. Schematics of the flow around a square cylinder confined in a channel.

4. Mathematical formulation

The governing equations (in their dimensionless forms) are the continuity, the x- and y-components of the Navier–Stokes and the thermal energy equations, assuming negligible dissipation and constant thermophysical properties, as given below.

Continuity:

$$\frac{\partial u}{\partial x} + \frac{\partial v}{\partial y} = 0 \tag{1}$$

x-momentum:

$$\frac{\partial u}{\partial t} + \frac{\partial uu}{\partial x} + \frac{\partial vu}{\partial y} = -\frac{\partial p}{\partial x} + \frac{1}{Re}\left(\frac{\partial^2 u}{\partial x^2} + \frac{\partial^2 u}{\partial y^2}\right) \tag{2}$$

y-momentum:

$$\frac{\partial v}{\partial t} + \frac{\partial uv}{\partial x} + \frac{\partial vv}{\partial y} = -\frac{\partial p}{\partial y} + \frac{1}{Re}\left(\frac{\partial^2 v}{\partial x^2} + \frac{\partial^2 v}{\partial y^2}\right) \tag{3}$$

Energy equation:

$$\frac{\partial T}{\partial t} + \frac{\partial (uT)}{\partial x} + \frac{\partial (vT)}{\partial y} = \frac{1}{Pe}\left(\frac{\partial^2 T}{\partial x^2} + \frac{\partial^2 T}{\partial y^2}\right) \tag{4}$$

The dimensionless boundary conditions may be written as follows:

- At inlet boundary, $u = [1 - (2\beta y)^2]$; $v = 0$; $T = 0$.
- At upper and lower boundary, $u = 0; v = 0; \frac{\partial T}{\partial y} = 0$.
- At square cylinder, $u = 0$; $v = 0$; $T = 1$ (constant temperature case) or $\frac{\partial T}{\partial n} = -1$ (constant heat flux case).
- At exit boundary, based on our experience [11–13,22,23], the Orlanski [24] boundary condition i.e. $\frac{\partial \phi}{\partial t} + U_c \frac{\partial \phi}{\partial x} = 0$ is employed here. Where the average streamwise velocity, $U_c = 2/3$ and Φ is the dependent variable, u or v or T.
- At the plane of symmetry at $y = 0, \frac{\partial u}{\partial y} = 0; v = 0; \frac{\partial T}{\partial y} = 0$.

Eqs. (1)–(4) together with the above-noted boundary conditions are solved to obtain $u(x, y)$, $v(x, y)$, $p(x, y)$ and $T(x, y)$, which in turn can be post-processed to obtain the values of the integral quantities and of the derived variables like stream function and vorticity.

5. Numerical methodology

5.1. Grid structure

The grid structure used in the present work is shown in Fig. 2(a) and (b). It shows the non-uniform grid structure for the whole of the computational domain (Fig. 2(a)) and an expanded view near the obstacle is shown in Fig. 2(b) for $\beta = 1/8$. It consists of five separate zones with uniform and non-uniform grid distribution having a close clustering of grid points in the regions of large gradients and coarser grids in the regions of low gradients. Overall, the grid distribution is uniform with a constant cell size, $\Delta = 0.25b$, in an outer region that extends beyond 4 units upstream and downstream of the cylinder in the x-direction. A much smaller grid size, δ, is clustered in an inner region around the cylinder over a distance of 1.5 units to adequately capture wake-wall interactions in both directions. The hyperbolic tangent function has been used for stretching the cell sizes between these limits of δ and Δ [25] in the x-direction. A fine grid of size, δ, is also clustered near the upper and lower walls of the channel to capture the wake-wall interactions. An algebraic expression [26] has been used for generating the grid points in the region 0.25 units away from the cylinder and the channel walls in the y-direction.

5.2. Numerical details

In the present work, the general finite volume method of Eswaran and Prakash [27] for complex 3D geometries on a non-staggered grid has been used here in its simplified form for 2D flows [28]. In brief, the semi-explicit method has been used to solve the unsteady Navier–

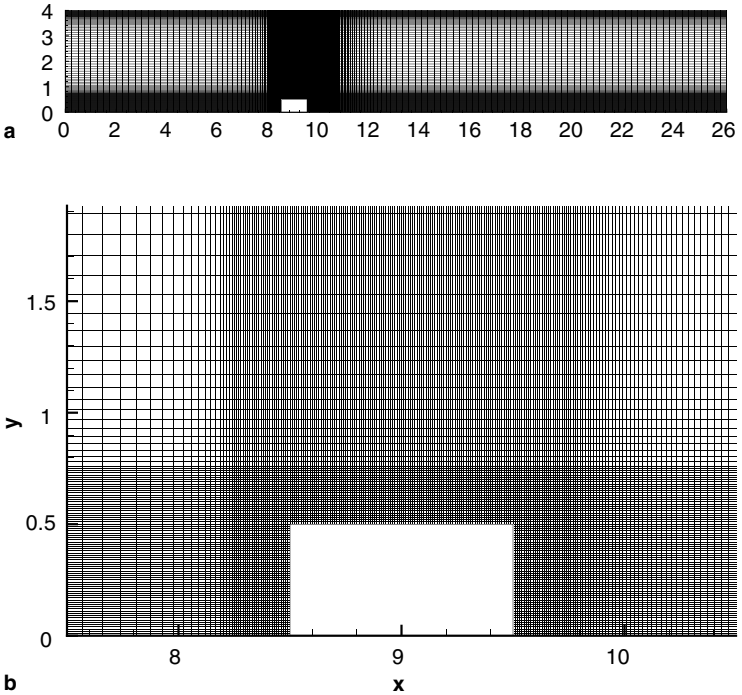

Fig. 2. Non-uniform computational grid structure with 323×150 grid points (a) and an expanded view near the obstacle (b) for $\beta = 1/8$.

Stokes equations in which the momentum equations are discretized in an explicit manner, with the exception of pressure gradient terms which are treated implicitly [29]. Consequently, the pressure–velocity coupling reduces to a Poisson equation for the pressure correction. The possible oscillations due to pressure–velocity decoupling on the collocated grid have been avoided by using the momentum interpolation scheme of Rhie and Chow [30]. Two steps are implemented at each time level: first, a predicted velocity is obtained from the discretized momentum equation using the previous time-level pressure field; the second corrector step consists of iterative solution of the pressure-correction equation and in obtaining the corresponding velocity corrections such that the final velocity field satisfies the continuity equation to the prescribed limit. The convective terms are discretized using QUICK [31] scheme while the diffusive terms are discretized using the central difference scheme.

The velocity fields obtained by solving the Navier–Stokes equations are used as an input to the energy equation. The explicit scheme has been used for the solution of the energy equation to obtain the temperature field.

5.3. Choice of numerical parameters

In order to ensure grid independence, four non-uniform grids (225×192, 283×260, 323×300 and 353×340, Table 1) were tested for the extreme values of Reynolds number of 45 and of Prandtl number of 50 for the blockage ratio of 1/4 (Fig. 3). The relative change in the values of C_D and Nu for the coarsest grid with respect to the finest grid are around 1.15%, and 0.24% (constant temperature case) and 0.79% (constant heat flux case), respectively. The difference in the values of C_D and Nu between the last two grid sizes are only about 0.22%, and 0.06% (constant temperature case) and 0.18% (constant heat flux case), respectively. It is also clear from Fig. 3 that the sensitivity of the front face Nusselt number is the highest with respect to the other faces of the cylinder. The difference in the value of Nu_f for the 225×192 grid is about 5.9% (constant temperature case) and 6.3% (constant heat flux case), and for 323×300, it is only 0.7% (constant temperature case) and 0.52% (constant heat flux case), as compared to the 353×340 grid, respectively. Therefore, the 323×300 grid size seems to be sufficiently fine to resolve the flow and heat transfer fields, and it has been used in all computations reported in this work.

Table 1
Details of four grids used at $Re=45$, $Pr=50$ and $\beta=1/4$

S. No.	Number of uniform CVs in the clustered region of $1.5b$ around the cylinder	Cell size (δ)	Grid size ($M\times N$)
1	72	0.0208	225×192
2	120	0.0125	283×260
3	150	0.0100	323×300
4	180	0.0083	353×340

6. Results and discussion

Extensive numerical computations have been carried out for $Re=1$, 2 and 5 to 45 in the steps of 5 for Peclet numbers ranging from 0.7 to 4000 for three blockage ratios ($\beta=1/8$, 1/6 and 1/4) for the symmetric top half of the channel. The numerical computations have also been carried out for the full domain configuration ($-L_2/2b\leqslant y\leqslant L_2/2b$) for the grid size of 323×300 to ensure that there exists a symmetric steady solution at least up to $Re=50$ for $\beta=1/8$, 1/6, 1/4. Additional test

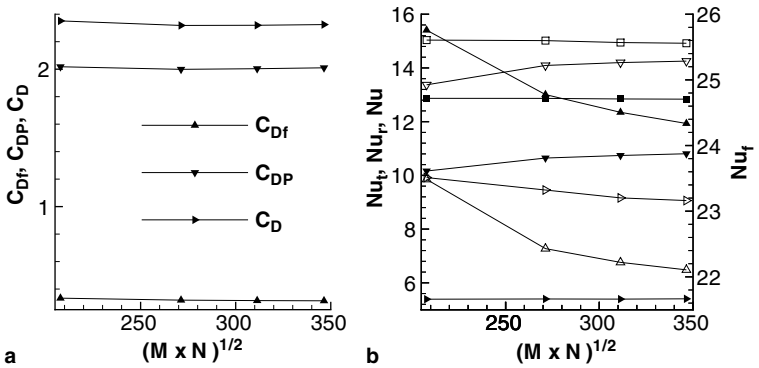

Fig. 3. Grid independence results at $Re=45$, $Pr=50$ and $\beta=1/4$ for the (a) individual and total drag coefficients (b) individual and overall average Nusselt number for the cylinder and each of its face. Filled and open symbols (b) correspond to the cases of constant cylinder temperature and constant heat flux, respectively, and the symbols □, △, ▽ and ▷ represent the average over the cylinder (Nu), front face (Nu_f), top face (Nu_t) and rear face (Nu_r), respectively.

Table 2
Comparison of L_r and C_D with the literature values ($\beta = 1/8$)

Source	$Re = 10$		$Re = 20$		$Re = 30$		$Re = 40$	
	L_r	C_D	L_r	C_D	L_r	C_D	L_r	C_D
Present	0.49	3.63	1.05	2.44	1.62	1.99	2.17	1.75
Breuer et al. [5]	0.49	3.64	1.04	2.50	1.60	2.00	2.15	1.70
Gupta et al. [22]	0.40	3.51	0.90	2.45	1.40	2.06	1.90	1.86

runs have also been carried out for $\beta = 1/5$ ($M \times N = 323 \times 300$) and $\beta = 1/2$ ($M \times N = 323 \times 200$) at $Re = 50$ (based on the average velocity) [13] to confirm the symmetry of the flow.

6.1. Validation of results

The numerical solution procedure has been benchmarked with standard results for the unconfined flow across a square cylinder reported elsewhere [23]. The present values of the recirculation length and drag coefficients are compared with those of Breuer et al. [5], Gupta et al. [22] in Table 2 for $Re = 10$, 20, 30 and 40 for $\beta = 1/8$. As Breuer et al. [5] have used FVM with a

Table 3
Comparison of L_r, C_D and Nu with the literature values for $\beta = 1/5$ and 1/2 at $Re = 50$

β	Source	L_r	C_D	Nu
1/5	Sharma and Eswaran [13]	2.687	3.622	3.578
	Present	2.689	3.603	3.554
1/2	Sharma and Eswaran [13]	1.563	13.299	4.922
	Present	1.561	13.208	4.874

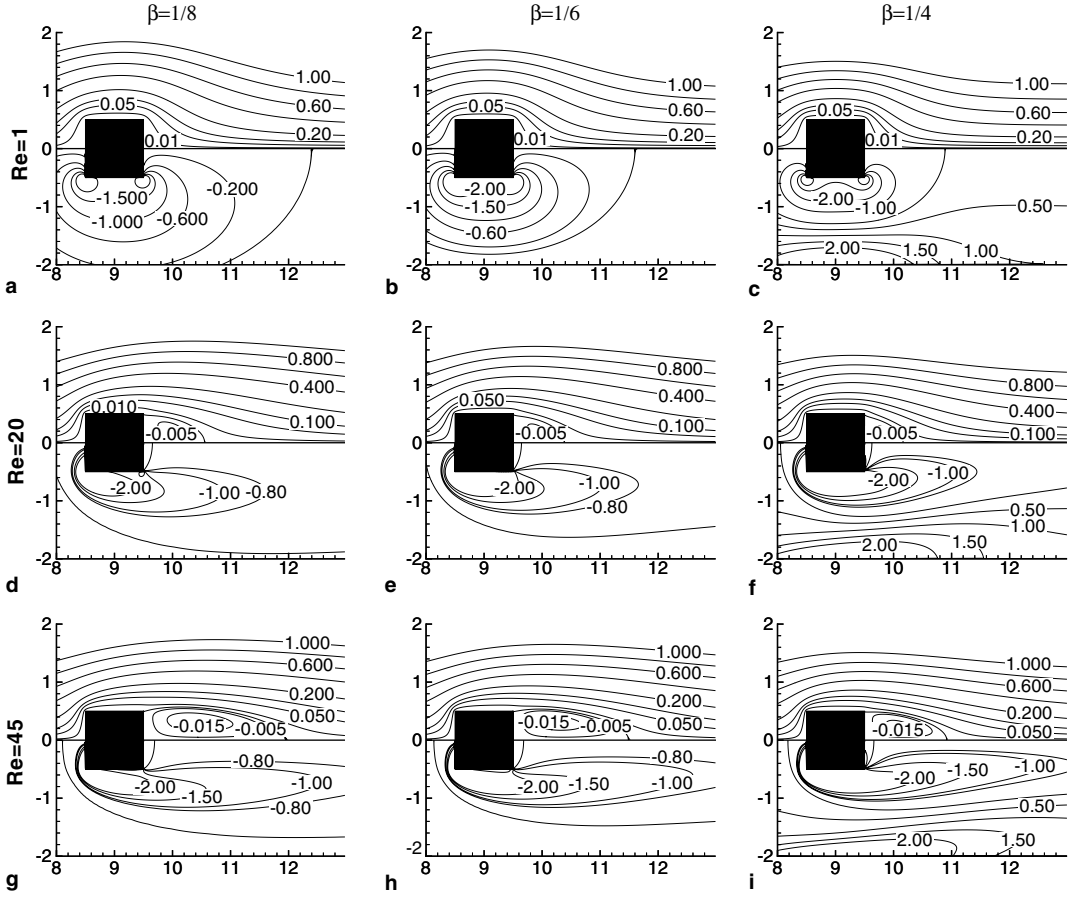

Fig. 4. Streamline and vorticity profiles (upper and lower half present the results for streamline and vorticity, respectively) for $Re = 1$, 20 and 45 at different blockage ratios.

clustering region of 100 CVs on the cylinder, in contrast to 10 CVs on the cylinder by Gupta et al. [22], the former results are likely to be more accurate. Table 3 presents a comparison of the present values of L_r, C_D and Nu ($Pr = 0.7$) with that of Sharma and Eswaran [13] at $Re = 50$ (based on average velocity) for $\beta = 1/5$ and 1/2. An excellent agreement is seen to exist between the present results and that of Breuer et al. [5] and of Sharma and Eswaran [13] in Tables 2 and 3, respectively. Mukhopadhyay et al. [16] computed the steady flow solution for $\beta = 1/4$ at $Re = 37$ (based on average velocity). They reported that the non-dimensional wake length to be ~2, while the corresponding value in the present case is 1.7. This discrepancy is very likely due to the differences of the grids used in these two studies (Mukhopadhyay et al. [16] have used only 4 or 8 CVs on each side of the obstacle as opposed to 100 CVs in the present case). Unfortunately, no experimental data is found in the literature for comparison for the inlet flow conditions and blockage ratios employed in this work. In addition to the above benchmarking, the general validity of the code used here has been checked for a few other flow problems: namely, the flow in a driven square cavity and the flow through a channel with backward-facing step in the 2D laminar flow regime; the results obtained in this work are in perfect agreement with the results available in the literature [32,33]. This further confirms the accuracy and reliability of the present numerical solution procedure.

Since the reliability and accuracy of the temperature (Table 3) field has also been established elsewhere [23], it is not repeated here.

6.2. Flow patterns

Fig. 4 presents representative flow patterns in the vicinity of a square cylinder by way of streamlines and vorticity profiles for $Re = 1$, 20 and 45 at blockage ratios of 1/8, 1/6 and 1/4. The streamline profiles are shown in the upper half of figures while the lower half shows the vorticity profiles. It is clearly seen in Fig. 4(a)–(c) that no flow separation occurs from the surface of the cylinder at $Re = 1$ as viscous forces dominate the flow. As the Reynolds number is gradually increased ($2 < Re \leqslant 45$), the flow separates at trailing edges of the cylinder and a closed recirculation region consisting of two symmetric vortices is observed behind the body (Fig. 4(d)–(i)). The size of these recirculation zones increases with an increase in the Reynolds number for a fixed value of the blockage ratio. It is also seen that the size of recirculation regions decreases with an increase in the blockage ratio for a fixed value of the Reynolds number. The

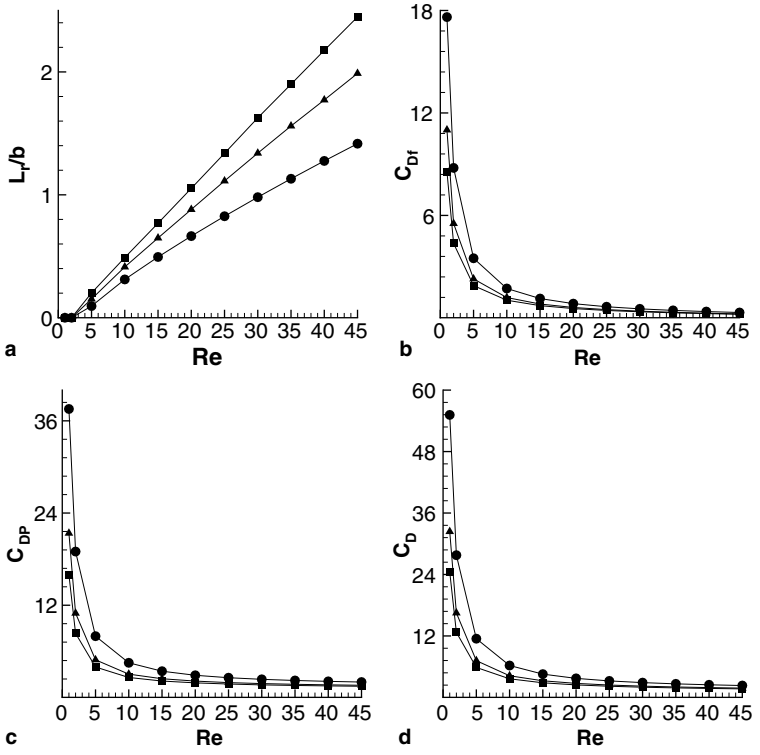

Fig. 5. Variation of recirculation length (a), friction drag (b), pressure drag (c) and total drag (d) coefficient with Reynolds number and blockage ratio, respectively: (■) $\beta = 1/8$, (▲) $\beta = 1/6$, (●) $\beta = 1/4$.

vorticity profiles can also be used to locate the separation points and to investigate the behaviour of the fluid flow, especially near the solid walls. For a fixed value of the blockage ratio, the vorticity contours seen to transit from being symmetrical at low Reynolds number to asymmetrical at high Reynolds numbers. Also, the magnitude of the vorticity is seen to increase with rising Reynolds number near the surface of the cylinder. On the other hand, for a fixed value of Reynolds number, the blockage ratio seems to have more pronounced effect at high Reynolds number than that at low Reynolds numbers. For instance, for $Re = 45$ and $\beta = 1/4$, the vorticity is seen to change sign near the wall.

6.3. Recirculation length

Fig. 5(a) shows the computed results of the non-dimensional recirculation length as a function of the Reynolds number and the blockage ratio. The length of the recirculation zone is seen to increase linearly with Reynolds number for a fixed blockage ratio, and to decrease with increasing blockage ratio for a fixed value of Reynolds number. Breuer et al. [5] proposed the following linear relationship between the recirculation length and Reynolds number for a fixed blockage ratio of 1/8 in the steady flow regime ($5 < Re < 60$):

$$L_r/b = -0.065 + 0.0554Re \tag{5}$$

The present results are within ±2% of the predictions of Eq. (5). The present results can be approximated somewhat better by the following equations:

For $\beta = 1/8$,

$$L_r/b = -0.0732 + 0.0563Re \tag{6}$$

For $\beta = 1/6$,

$$L_r/b = -0.0454 + 0.0457Re \tag{7}$$

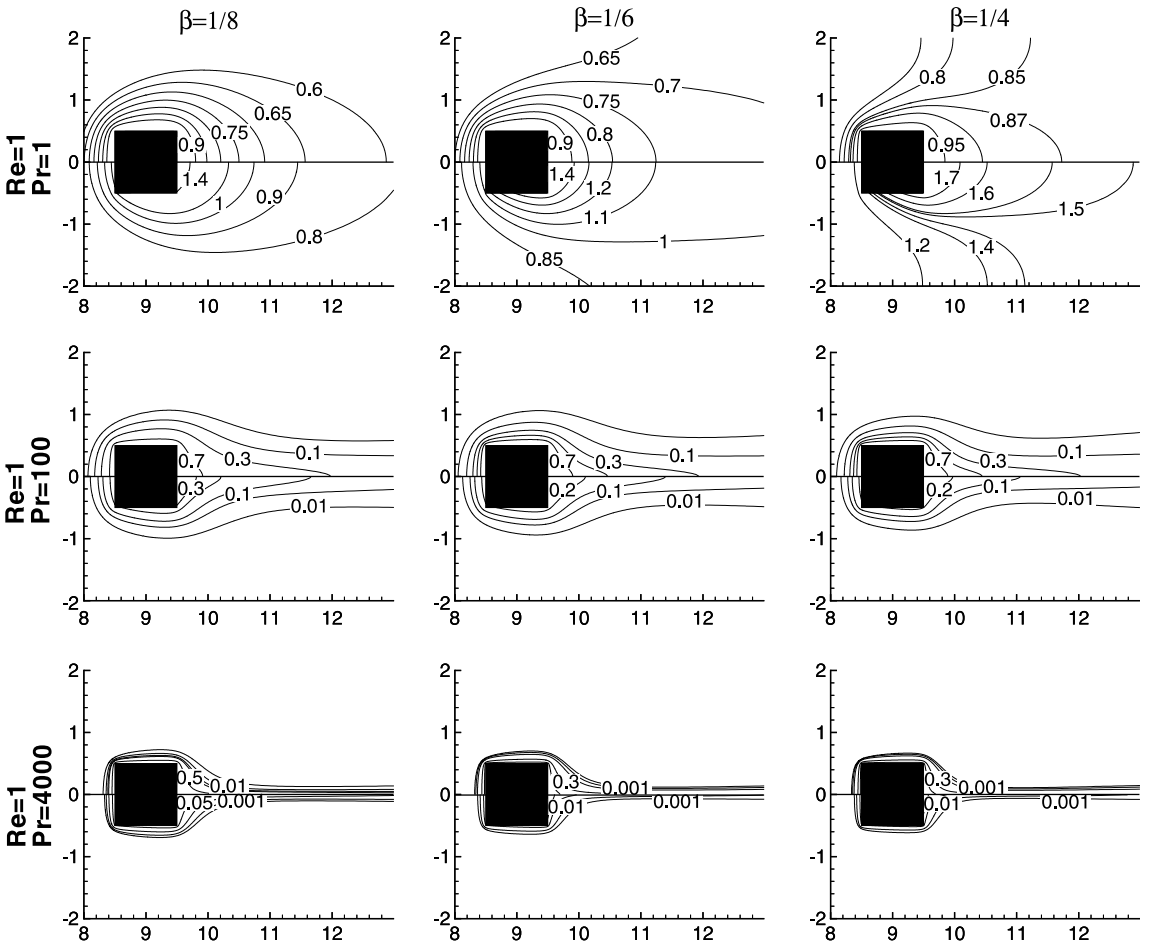

Fig. 6. Isotherms (upper and lower half present the results for constant cylinder temperature and constant heat flux cases, respectively) for $Re = 1$ and $Pr = 1$, 100 and 4000 at different blockage ratios.

For $\beta = 1/4$,

$$L_r/b = -0.0145 + 0.0326Re \quad (8)$$

These correlations have maximum deviations of 0.65%, 1.45% and 4.1% for $\beta = 1/8$, 1/6 and 1/4, respectively, from the computed results in the Reynolds number range $5 < Re \leqslant 45$. Also, since the fitted constants in Eqs. (6)–(8) show regular variation with β whence these results can readily be interpolated for the intermediate values of β. Intuitively, one would expect this dependence to become non-linear at some value of β. Admittedly, the results for $\beta = 1/4$ do show slightly non-linear dependence, but Eq. (8) still describes these results within $\pm 4.1\%$ which is comparable to a second-degree polynomial fit to the data.

6.4. Drag coefficient

The drag force exerted on the obstacle is made up of two components: viscous drag coefficient ($C_{Df} = \frac{F_{Df}}{\frac{1}{2}\rho U_{max}^2 b}$) and pressure drag coefficient ($C_{DP} = \frac{F_{DP}}{\frac{1}{2}\rho U_{max}^2 b}$) and the total drag coefficient, $C_D = C_{Df} + C_{DP}$. Fig. 5(b)–(d) shows the variation of these components with Reynolds number for three values of β. As expected, the values of the individual and total drag coefficients show inverse dependence on the Reynolds number for a fixed blockage ratio. At low Reynolds numbers, drag coefficients depend strongly on the Reynolds number (slope of ~ -1), as the viscous forces play a dominant role in the steady flow regime. It is also observed that drag coefficients increase as the extent of channel confinement (β) increases for a fixed Reynolds number.

6.5. Isotherm patterns

Fig. 6 presents the representative isotherms close to the square cylinder for $Re = 1$ at different values of Prandtl numbers ($Pr = 1$, 100 and 4000) for the blockage ratios of 1/8, 1/6 and 1/4, respectively. The top half shows

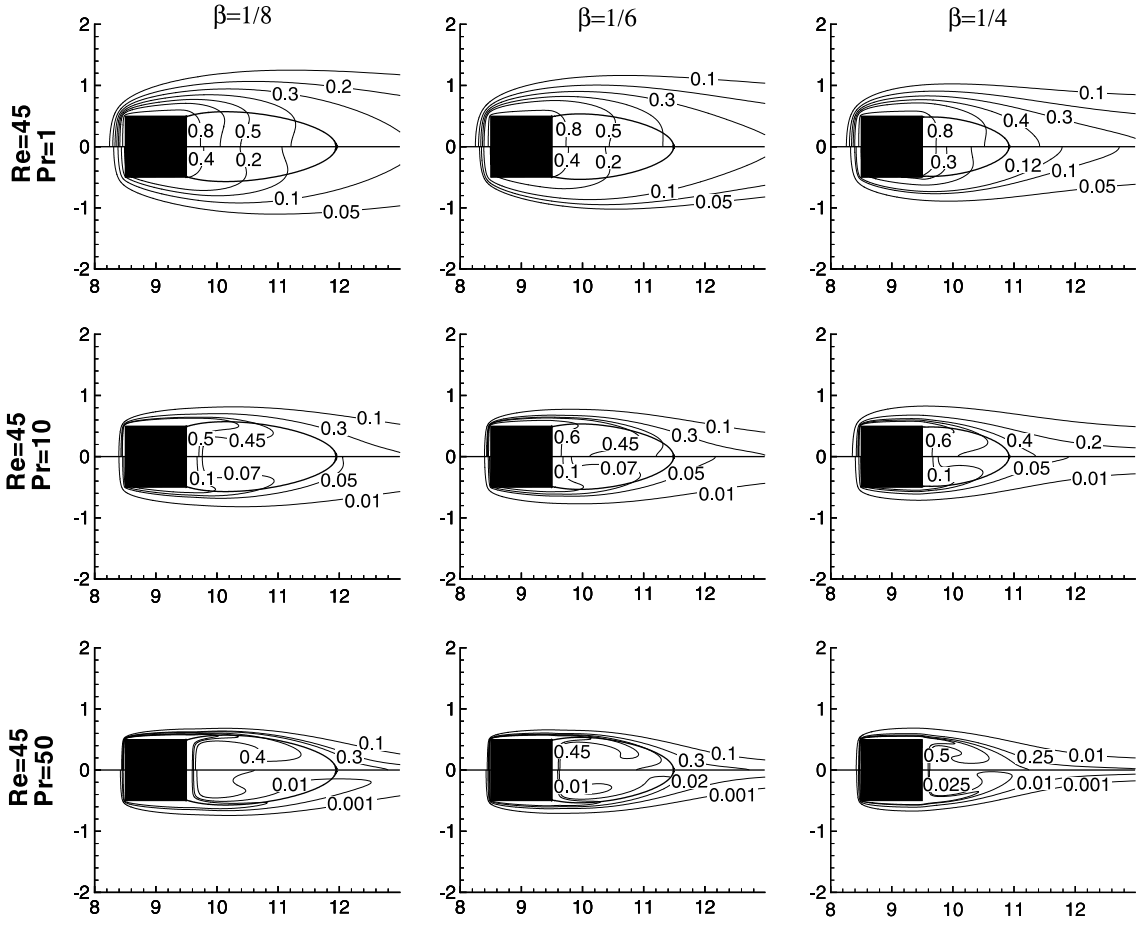

Fig. 7. The streamline representing the closed near wake (shown by a thick line) and isotherms (upper and lower half present the results for constant cylinder temperature and constant heat flux cases, respectively) for $Re = 45$ and $Pr = 1$, 10 and 50 at different blockage ratios.

the isotherms for the isothermal cylinder whereas the lower half shows the isotherms for the cylinder with constant heat flux condition. For a fixed value of β and Re, as expected, the thermal boundary layer thickness decreases rapidly as the value of Pr is progressively increased from 1 to 4000. On the other hand, for fixed values of Re and Pr, the isotherms are increasingly distorted by the presence of the adiabatic walls, e.g., see the results for $\beta = 1/4$ at $Re = 1$ and $Pr = 1$. As the value of Pr increases this effect diminishes, presumably due to the thinning of the thermal boundary layer. Fig. 7 shows the streamline enclosing the closed near wake (shown by a thick line) and isotherms near the square cylinder for $Re = 45$ at various Prandtl numbers ($Pr = 1$, 10 and 50) for the blockage ratios of 1/8, 1/6 and 1/4, respectively. The isotherms for the constant temperature condition are again shown in the upper half of the figures while the lower half depicts that for the constant heat flux condition. It is clearly seen from these figures that the front surface has the maximum crowding of the temperature contours, indicating the highest Nusselt number as compared to the other faces of the cylinder, since the boundary layer starts from this surface. Fig. 6 also shows the decay of temperature field with an increase in the Prandtl numbers for both thermal boundary conditions at different blockage ratios as the thickness of thermal boundary layer decreases with increasing Prandtl number. As the Reynolds number increases, the length of the recirculation region increases and also the crowding of the temperature contours near the rear surface of the cylinder increases with an increase in the Prandtl number, for both thermal boundary conditions. Also, the clustering of isotherms increases with the increasing Reynolds and/or Prandtl number. This is due to the increased circulation of large amount of fluid with increasing Reynolds number and/or the decreasing thickness of the thermal boundary layer with increasing Prandtl number. Fig. 7 also shows the diminishing effect of the bounding walls at high Reynolds number and/or Prandtl number.

6.6. Local Nusselt number

In this study, the local Nusselt number is defined as $-\frac{\partial T}{\partial n}$ and $\frac{1}{T_w}$ for the two thermal boundary conditions, respectively. Due to the singularity at the corner of the obstacle, special attention was paid to the role of the grid size on the value of the local Nusselt number at each corner of the obstacle. The peak value of the local Nusselt number at the corner point was seen to progressively decrease as the grid becomes coarser. In spite of such strong dependence of the corner point values on grid

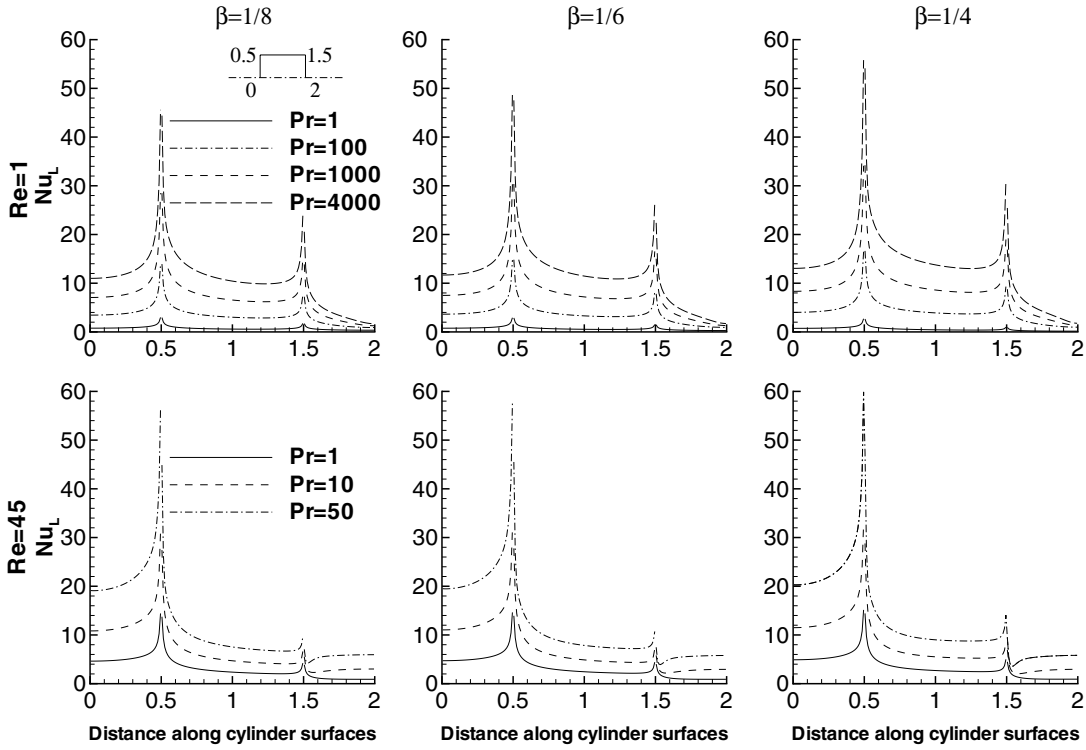

Fig. 8. Local Nusselt number variation along the cylinder surface (from the front stagnation point to the rear stagnation point) for $Re = 1$ and 45 at different blockage ratios and Prandtl numbers for constant cylinder temperature case.

interval, owing to the vanishing small heat transfer area, the surface average values of the Nusselt number are quite insensitive to the corner values. However, as mentioned previously, the grid size of 323×300 is sufficiently fine to obtain results that are essentially grid independent.

6.6.1. Constant temperature case (isothermal obstacle)

The effect of blockage ratio on the variation of the local Nusselt number along the cylinder surface for the top half of the square cylinder at $Re = 1$ and at $Re = 45$ for various values of Prandtl numbers is shown in Fig. 8. It is clear from these plots that the Nusselt number increases with the increasing values of the Reynolds number and/or Prandtl number at each blockage ratio studied here. The increase in the Nusselt number increases due to the blockage ratio stems primarily from the sharpening of the temperature gradients. Also, as expected each corner of the square cylinder shows high Nusselt number due to the large temperature gradient normal to the surface of the obstacle. These plots also show that the local Nusselt number increases towards the corner on the front face of the square cylinder as there is a maximum crowding of isotherms at this face. On the top surface of the cylinder, there exists a minimum as the Nusselt number increases near the trailing edge of the cylinder. On the rear surface of the cylinder, there is a local minimum at the axis of symmetry at $Re = 1$ and near the corner at $Re = 45$.

6.6.2. Constant heat flux case

The effect of blockage on the variation of local Nusselt number for the top half of the square cylinder (the other half is symmetric) along the cylinder surfaces at $Re = 1$ and 45 for various values of Prandtl numbers for the constant heat flux case is shown in Fig. 9 for $\beta = 1/8$, 1/6 and 1/4. These plots reveal qualitatively similar features as seen above for the constant temperature condition case.

6.7. Average Nusselt number

The average Nusselt number for each surface (Nu_f, Nu_r, Nu_t) of the square cylinder is obtained by averaging the local Nusselt number over the each face of the obstacle. Finally, the overall mean value of the cylinder Nusselt number (Nu) is obtained by averaging the averaged Nusselt number for each surface of the cylinder.

6.7.1. Constant temperature case

The effect of blockage ratio on the variation of the average Nusselt number for the square cylinder, and

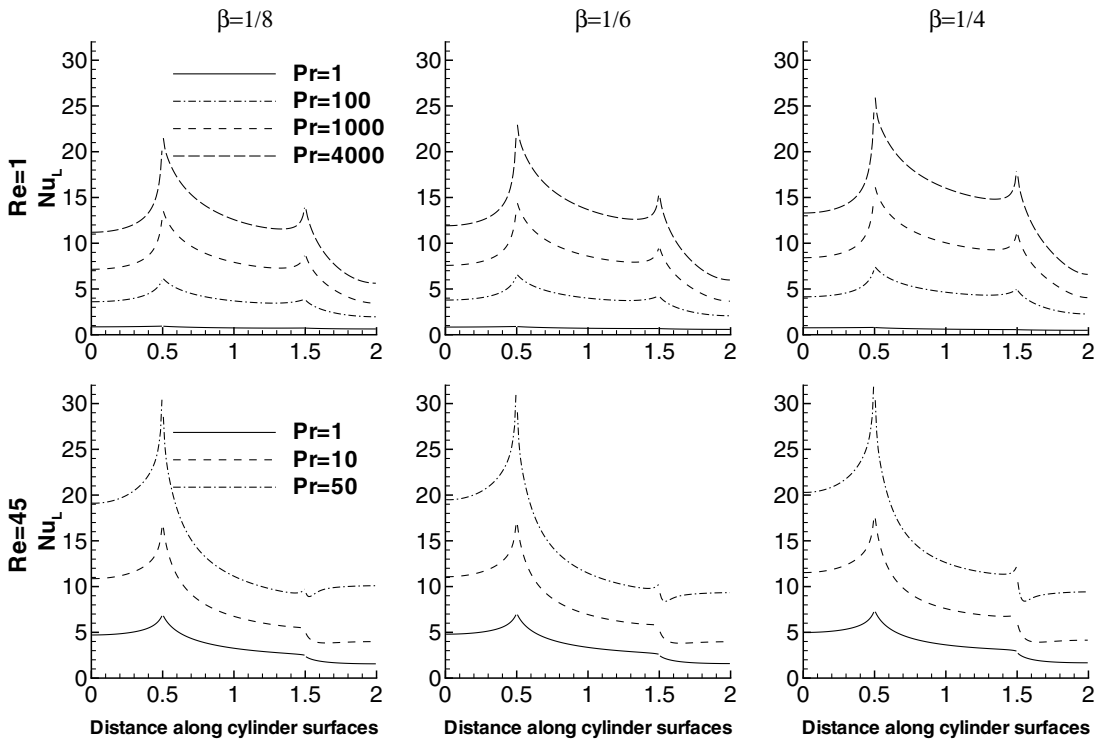

Fig. 9. Local Nusselt number variation along the cylinder surface (from the front stagnation point to the rear stagnation point) for $Re = 1$ and 45 at different blockage ratios and Prandtl numbers for constant heat flux case.

each of its faces, as a function of Reynolds number for various Prandtl numbers is shown in Figs. 10–12. These figures show that the front surface has the highest average Nusselt number, the top and bottom surface value is intermediate, followed by the rear surface. It is also seen that the average Nusselt number for the cylinder and each of its faces increases with increasing Reynolds and/or Prandtl numbers for all blockage ratios investigated here. With an increase in the blockage ratio, the average Nusselt number for the cylinder and each of its faces increases because the wake length decreases.

From an application standpoint, it is convenient to correlate the present heat transfer results by simple expressions. Simple dimensional considerations suggest the Nusselt number to be a function of the Reynolds number, Prandtl number, blockage ratio and the nature of the thermal boundary condition. For a fixed value of the blockage ratio and the type of thermal boundary condition, the average Nusselt number varies approximately linearly on a logarithmic scale with respect to Reynolds and Prandtl number over the Peclet number range 0.7–4000.

By analogy with the results for the unconfined flow past a square cylinder [23], it is customary to introduce the Colburn heat transfer factor (j), as follows:

$$j = Nu/(Re \times Pr^{1/3}) \tag{9}$$

The use of j factor collapses the results for different values of the Prandtl number on to one curve and it can also be used to predict the heat transfer rates at different Reynolds numbers. This form of presentation also exploits the usual analogy between heat and mass transfer thereby allowing the use of Eqs. (10)–(12) to estimate the corresponding mass transfer coefficient also. A least-squares method has been used to get a linear fit on a log–log plot of $Nu/Pr^{1/3}$ versus Re for various values of Re and Pr, the following expressions (10)–(12) can be used to evaluate Nu for different values of β.

Fig. 13(a)–(c) show the present results in terms of the j factor for the constant temperature case at three values of the blockage ratios. The results corresponding to different values of Pr are seen to collapse on to one line corresponding to each value of β for the Reynolds number range $1 \leqslant Re \leqslant 45$ with some deviations at $Re = 1$

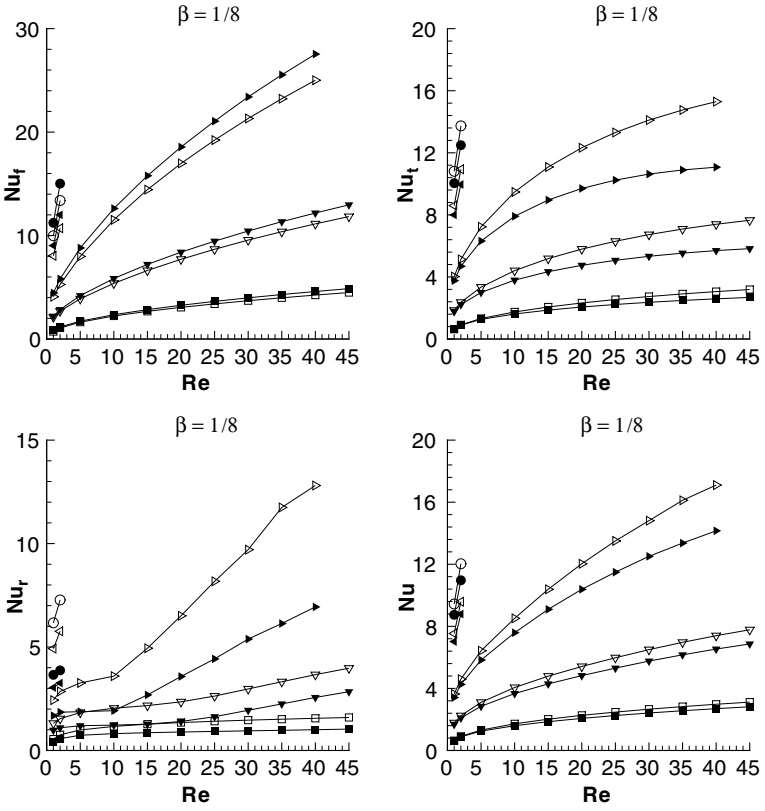

Fig. 10. Average Nusselt number for the cylinder and each of its faces as a function of Reynolds and Prandtl number for constant temperature (filled symbols) and constant heat flux (opened symbols) cases ($\beta = 1/8$): (□) $Pr = 0.7$, (▽) $Pr = 10$, (▷) $Pr = 100$, (◁) $Pr = 1000$, (○) $Pr = 2000$.

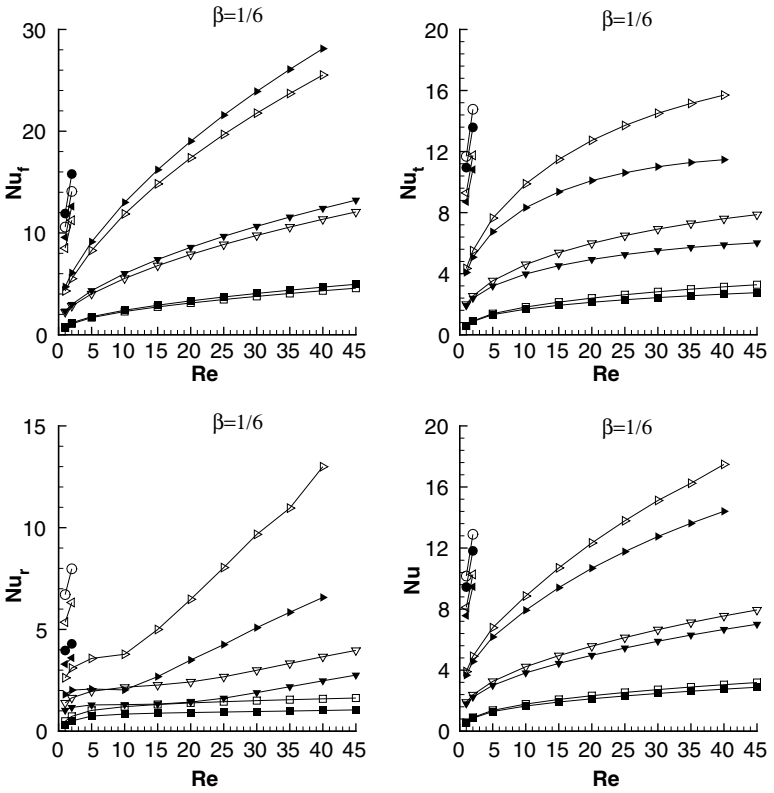

Fig. 11. Average Nusselt number for the cylinder and each of its faces as a function of Reynolds and Prandtl number for constant temperature (filled symbols) and constant heat flux (opened symbols) cases ($\beta = 1/6$). Key to symbols is same as in Fig. 10.

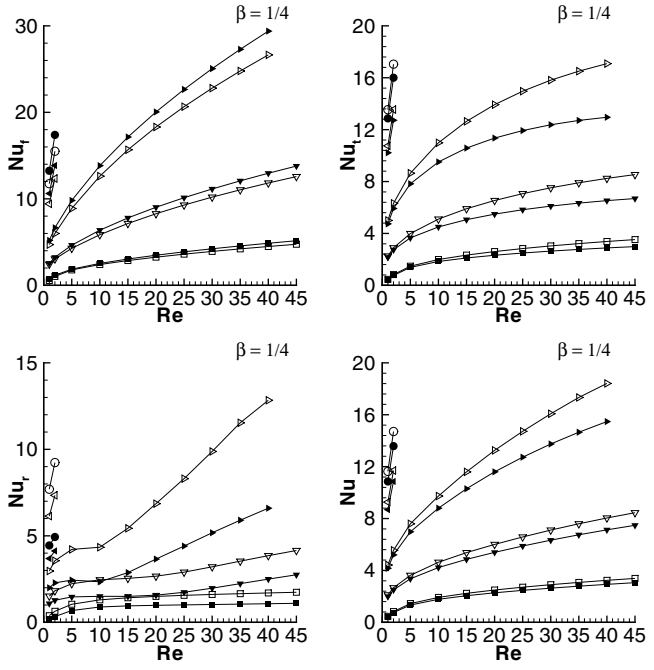

Fig. 12. Average Nusselt number for the cylinder and each of its faces as a function of Reynolds and Prandtl number for constant temperature (filled symbols) and constant heat flux (opened symbols) cases ($\beta = 1/4$). Key to symbols is same as in Fig. 10.

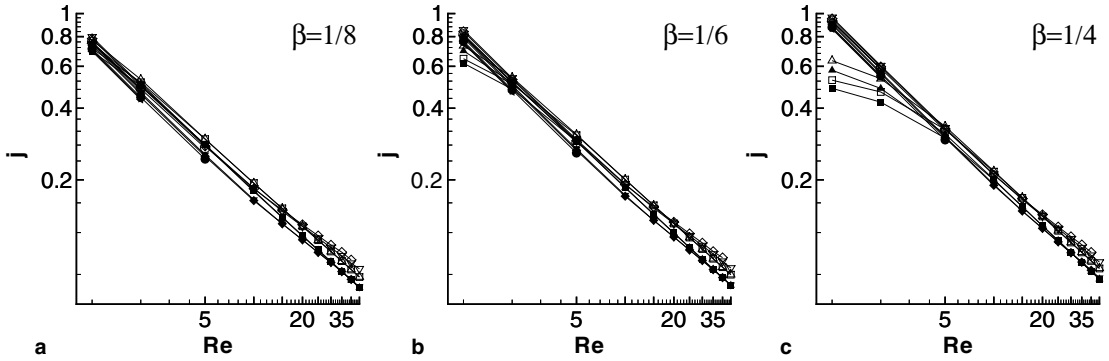

Fig. 13. The Colburn j factor as a function of Reynolds number at various Prandtl numbers for constant temperature (filled symbols) and constant heat flux (opened symbols) cases at different blockage ratios, respectively: (□) $Pr = 0.7$, (△) $Pr = 1$, (▽) $Pr = 50$, (◇) $Pr = 100$, (○) $Pr = 500$, (▷) $Pr = 1000$, (◁) $Pr = 2000$.

for $\beta = 1/6$ and at $Re = 1$ and 2 for $\beta = 1/4$ (Fig. 13). The following simple expressions correlate the present results adequately:

For $\beta = 1/8$,

$$j = 0.7155 \times Re^{-0.6136} \tag{10}$$

For $\beta = 1/6$,

$$j = 0.7567 \times Re^{-0.6225} \tag{11}$$

For $\beta = 1/4$,

$$j = 0.8286 \times Re^{-0.6266} \tag{12}$$

These correlations show the heat transfer rates are low at low Reynolds numbers and high at high Reynolds numbers. These expressions have average deviations of the order of 3% for $\beta = 1/8$, 1/6 and of 4% for $\beta = 1/4$ for the Reynolds number range $1 \leqslant Re \leqslant 45$ and the Peclet number range $0.7 \leqslant Pe \leqslant 4000$, respectively; the maximum deviations are about 10%, 8% and 4% for $\beta = 1/8$, 1/6 and 1/4 which are slightly larger than that associated with Eqs. (13)–(15) for $\beta = 1/8$ and 1/6, respectively.

6.7.2. Constant heat flux case

The effect of blockage on the variation of average Nusselt number for the square cylinder, and each of its faces, as a function of Reynolds number for various Prandtl numbers for the constant heat flux case is shown in Figs. 10–12. The dependence of the average Nusselt number on the Reynolds and Prandtl numbers and blockage ratio seen in these figures is qualitatively similar to that observed for the condition of constant temperature. As expected, the overall mean values are some what larger than those obtained for the constant temperature case at the same values of β, Pr and Re.

Fig. 13(a)–(c) also show the functional dependency of the j factor on the flow and heat transfer parameters for the constant heat flux condition. These results are also seen to collapse on to one curve for different values of Prandtl number in the steady flow regime. The following expressions give reasonable correlations of the numerical data:

For $\beta = 1/8$,

$$j = 0.7579 \times Re^{-0.5929} \tag{13}$$

For $\beta = 1/6$,

$$j = 0.8015 \times Re^{-0.6022} \tag{14}$$

For $\beta = 1/4$,

$$j = 0.8809 \times Re^{-0.6094} \tag{15}$$

These expressions have average deviations of the order of 3% for $\beta = 1/8$, 1/6 and of 4% for $\beta = 1/4$, respectively; the maximum deviation is about 8% for $\beta = 1/8$, 1/6 and of 7% for $\beta = 1/4$, respectively. However, the results for low Reynolds number ($Re \leqslant 2$) and small Prandtl numbers ($\leqslant 1$) deviate significantly from Eqs. (13)–(15), as in other correlations presented previously. These deviations of the computed results with the correlations at low Re and small Pr is due to no wake formation for $Re \leqslant 2$ behind the obstacle, as a result of which conduction is more dominant here. As expected, the presence of confining walls enhances heat transfer depending upon the value of the Peclet number and the blockage ratio. Broadly, lower is the Reynolds number, greater is the enhancement. Similarly, it also rises with the increasing value of β. For instance, for $Pe = 4000$ ($Re = 1$ and $Pr = 4000$) and $\beta = 1/4$, the gain in heat transfer as compared to the unconfined case is of the order of 47%.

7. Conclusions

The effect of Peclet number ($0.7 \leqslant Pe \leqslant 4000$) and blockage ratio ($\beta = 1/8$, 1/6 and 1/4) on the flow and

heat transfer characteristics of a square cylinder confined in a planar channel has been investigated in the Reynolds number range $1 \leqslant Re \leqslant 45$ in the 2D steady flow regime. The effect of the type of thermal boundary condition at the cylinder surface, i.e., constant cylinder temperature and constant heat flux, on the rate of heat transfer has also been studied. Broadly speaking, the use of the constant heat flux boundary condition yields slightly higher values of the Nusselt number than those for the constant temperature case under otherwise identical conditions of β, Re and Pr. The difference in the computed values of the average Nusselt number for the two types of thermal boundary conditions increases as the Prandtl number is increased for fixed values of the Reynolds number for all blockage ratios. Also, this difference increases with the increasing Reynolds number for fixed value of Prandtl number for all blockage ratios. The local Nusselt number variation on each face of the cylinder has been determined. Further insights into the role of blockage ratio, Reynolds and Prandtl number on the detailed flow and temperature fields have been provided by including streamline, vorticity and constant temperature contour plots. The average Nusselt number increases monotonically with an increase in the Reynolds number and/or Prandtl number. Finally, heat transfer correlations have been obtained for the constant temperature and constant heat flux cases on the solid square cylinder in crossflow over the range of physical parameters considered in this study.

References

[1] M.M. ZdravkovichFlow Around Circular Cylinders: Fundamentals, vol. 1, Oxford University Press, New York, 1997.

[2] M.M. ZdravkovichFlow Around Circular Cylinders: Applications, vol. 2, Oxford University Press, New York, 2003.

[3] V.T. Morgan, The overall convective heat transfer from smooth circular cylinders, Adv. Heat Transfer 11 (1975) 199–264.

[4] R.A. Ahmad, Steady-state numerical solution of the Navier–Stokes and energy equations around a horizontal cylinder at moderate Reynolds numbers from 100 to 500, Heat Transfer Eng. 17 (1) (1996) 31–81.

[5] M. Breuer, J. Bernsdorf, T. Zeiser, F. Durst, Accurate computations of the laminar flow past a square cylinder based on two different methods: lattice-Boltzmann and finite-volume, Int. J. Heat Fluid Flow 21 (2000) 186–196.

[6] W.-B. Guo, N.-C. Wang, B.-C. Shi, Z.-L. Guo, Lattice-BGK simulation of a two-dimensional channel flow around a square cylinder, Chin. Phys. 12 (1) (2003) 67–74.

[7] A. Okajima, Strouhal numbers of rectangular cylinders, J. Fluid Mech. 123 (1982) 379–398.

[8] K.M. Kelkar, S.V. Patankar, Numerical prediction of vortex shedding behind a square cylinder, Int. J. Numer. Methods Fluids 14 (1992) 327–341.

[9] A. Sohankar, L. Davidson, C. Norberg, Numerical simulation of unsteady flow around a square two-dimensional cylinder, in: Proceedings of the 12th Australian Fluid Mechanics Conference, Sydney, Australia, 1995, pp. 517–520.

[10] R. Franke, W. Rodi, B. Schonung, Numerical calculation of laminar vortex-shedding flow past cylinders, J. Wind Eng. Ind. Aerodyn. 35 (1990) 237–257.

[11] A. Sharma, V. Eswaran, Heat and fluid flow across a square cylinder in the two-dimensional laminar flow regime, Numer. Heat Transfer Part A 45 (2004) 247–269.

[12] A. Sharma, V. Eswaran, Effect of adding and opposing buoyancy on the heat and fluid flow across a square cylinder at $Re = 100$, Numer. Heat Transfer Part A 45 (2004) 601–624.

[13] A. Sharma, V. Eswaran, Effect of channel-confinement on the two-dimensional laminar flow and heat transfer across a square cylinder, Numer. Heat Transfer Part A 47 (2005) 79–107.

[14] J. Robichaux, S. Balachandar, S.P. Vanka, Three-dimensional floquet instability of the wake of square cylinder, Phys. Fluids 11 (3) (1999) 560–578.

[15] R.W. Davis, E.F. Moore, L.P. Purtell, A numerical–experimental study of confined flow around rectangular cylinders, Phys. Fluids 27 (1) (1984) 46–59.

[16] A. Mukhopadhyay, G. Biswas, T. Sundararajan, Numerical investigation of confined wakes behind a square cylinder in a channel, Int. J. Numer. Methods Fluids 14 (1992) 1473–1484.

[17] K. Suzuki, H. Suzuki, Unsteady heat transfer in a channel obstructed by an immersed body, in: C.L. Tien (Ed.), Annual Review of Heat Transfer, vol. 5, Begell House, New York, 1994, pp. 177–206.

[18] A. Valencia, Heat transfer enhancement in a channel with a built-in square cylinder, Int. Comm. Heat Mass Transfer 22 (1) (1995) 47–58.

[19] J. Bernsdorf, T. Zeiser, G. Brenner, F. Durst, Simulation of a 2D channel flow around a square obstacle with lattice-Boltzmann (BGK) automata, in: Proceedings of the Seventh International Conference on the Discrete Simulation of Fluids, University of Oxford, 14–18 July 1998, International Journal of Modern Physics C 9 (8) (1998) 1129–1141.

[20] S. Turki, H. Abbassi, S.B. Nasrallah, Effect of the blockage ratio on the flow in a channel with a built-in square cylinder, Comput. Mech. 33 (2003) 22–29.

[21] S. Turki, H. Abbassi, S.B. Nasrallah, Two-dimensional laminar fluid flow and heat transfer in a channel with a built-in heated square cylinder, Int. J. Thermal Sci. 42 (2003) 1105–1113.

[22] A.K. Gupta, A. Sharma, R.P. Chhabra, V. Eswaran, Two-dimensional steady flow of a power law fluid past a square cylinder in a plane channel: momentum and heat transfer characteristics, Ind. Eng. Chem. Res. 42 (2003) 5674–5686.

[23] A.K. Dhiman, R.P. Chhabra, A. Sharma, V. Eswaran, Effects of Reynolds and Prandtl numbers on the heat transfer across a square cylinder in the steady flow regime, Num. Heat Transfer Part A (2005), in press.

[24] I. Orlanski, A simple boundary condition for unbounded hyperbolic flows, J. Comput. Phys. 21 (1976) 251–269.

[25] J.F. Thompson, Z.U.A. Warsi, C.W. Mastin, Numerical Grid Generation: Foundations and Applications, Elsevier Science, New York, 1985, pp. 305–310.
[26] K.A. Hoffmann, Computational Fluid Dynamics for Engineers, Engineering Education System, Austin, TX, 1989.
[27] V. Eswaran, S. Prakash, A finite volume method for Navier–Stokes equations, in: Proceedings of the Third Asian CFD Conference, Bangalore, India, vol. 1, 1998, pp. 127–136.
[28] A. Sharma, Numerical investigation of unconfined and channel-confined flow across a square cylinder with forced and mixed convection heat transfer, Ph.D. Thesis, Indian Institute of Technology Kanpur, India, 2003.
[29] A. Sharma, V. Eswaran, in: K. Muralidhar, T. Sundararajan (Eds.), A Finite Volume Method: In Computational Fluid Flow and Heat Transfer, Narosa Publishing House, New Delhi, 2003, pp. 445–482.
[30] C.M. Rhie, W.L. Chow, A numerical study of the turbulent flow past an isolated aerofoil with trailing edge separation, AIAA J. 21 (1983) 1525–1532.
[31] B.P. Leonard, A stable and accurate convective modeling procedure based on quadratic upstream interpolation, Comput. Methods Appl. Mech. Eng. 19 (1979) 59–98.
[32] U. Ghia, K.N. Ghia, C.T. Shin, High-*Re* solutions for incompressible flow using the Navier–Stokes equations and a multigrid method, J. Comput. Phys. 48 (1982) 387–411.
[33] A.K. Verma, A finite volume solution method for fluid flow problems, Ph.D. Thesis, Indian Institute of Technology Kanpur, India, 1997.